

# CO<sub>2</sub>-Responsive Water-Soluble Conjugated Polymers for *In Vitro* and *In Vivo* Biological Imaging

Chih-Chia Cheng,\* You-Cheng Lai, Yeong-Tarng Shieh, Yi-Hsuan Chang, Ai-Wei Lee, Jem-Kun Chen, Duu-Jong Lee, and Juin-Yih Lai



Cite This: <https://dx.doi.org/10.1021/acs.biomac.0c01336>



Read Online

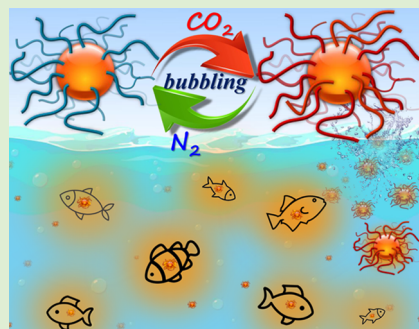
ACCESS |

Metrics & More

Article Recommendations

Supporting Information

**ABSTRACT:** Water-soluble conjugated polymers (WCPs) composed of a hydrophobic polythiophene main chain with hydrophilic tertiary amine side-chains can directly self-assemble into sphere-like nano-objects in an aqueous solution due to phase separation between the hydrophilic and hydrophobic segments of the polymeric structure. Due to the presence of gas-responsive tertiary amine moieties in the spherical structure, the resulting polymers rapidly and reversibly tune their structural features, surface charge, and fluorescence performance in response to alternating carbon dioxide (CO<sub>2</sub>) and nitrogen (N<sub>2</sub>) bubbling, which leads to significantly enhanced fluorescence and surface charge switching properties and a stable cycle of on and off switching response. *In vitro* studies confirmed that the CO<sub>2</sub>-treated polymers exhibited extremely low cytotoxicity and enhanced cellular uptake ability in normal and tumor cells, and thus possess significantly improved fluorescence stability, distribution, and endocytic uptake efficiency within cellular organisms compared to the pristine polymer. More importantly, *in vivo* assays demonstrated that the CO<sub>2</sub>-treated polymers displayed excellent biocompatibility and high fluorescence enhancement in living zebrafish, whereas the fluorescence intensity and stability of zebrafish incubated with the pristine polymer decreased linearly over time. Thus, these CO<sub>2</sub> and N<sub>2</sub>-responsive WCPs could potentially be applied as multifunctional fluorescent probes for *in vivo* biological imaging.



## INTRODUCTION

Water-soluble conjugated polymers (WCPs) have attracted considerable attention over the last decade due to global environmental problems related to the use of organic solvents. WCPs dissolve easily in environmentally friendly water-based solvents,<sup>1–3</sup> and meet a wide range of requirements for environmental safety and sustainable development.<sup>4–8</sup> By altering the water solubility of the hydrophobic conjugated polymer, WCPs in an aqueous solution can further self-assemble into hierarchical nanostructures to fabricate water-soluble fluorescent nanoprobes. The spontaneous self-assembly behavior of WCPs can prevent issues related to hydrophobic interaction-induced dynamic aggregation and precipitation, and thus enhances their structural stability and the balance between hydrophilic and hydrophobic properties.<sup>9–12</sup> In terms of the unique feature of the self-assembly behavior, the nanostructure of self-assembled WCPs strongly influences their emission properties and results in well-controlled fluorescent performance with different colors of emission; therefore, WCPs have been widely used for live-cell imaging applications *in vitro* and *in vivo*.<sup>13–17</sup> However, several drawbacks still limit the biomedical application of WCP systems *in vitro* and *in vivo*, including their multistep preparation procedures and lack of long-term fluorescent stability and multiple-response capability under intracellular conditions, which lead to insufficient fluorescence brightness and labeling and complicate dynamic

cell tracking *in vivo*.<sup>18–21</sup> To overcome these obstacles and significantly improve the physical properties of WCPs in an aqueous solution and biological media, it is necessary to obtain an intelligent multifunctional WCP system that exhibits multiresponsiveness to environmental stimuli and enhanced structural stability and fluorescence efficiency in complex biological microenvironments; such developments may potentially generate highly stable fluorescent probes for *in vitro* and *in vivo* bioimaging applications.

Stimuli-responsive polymers represent a potentially effective and efficient strategy to confront the issues mentioned above. Stimuli-responsive polymer systems have attracted significant research attention in recent decades, as the physical properties of the functional polymers can be manipulated by changing their internal and external environments.<sup>22–26</sup> The widely studied stimuli that activate these polymeric systems include temperature,<sup>27,28</sup> pH,<sup>29,30</sup> light,<sup>28,31</sup> magnetic field,<sup>32</sup> and gas.<sup>22–26</sup> Adding or removing gases can induce physical changes by inducing a polymer to undergo phase transitions

Received: September 16, 2020

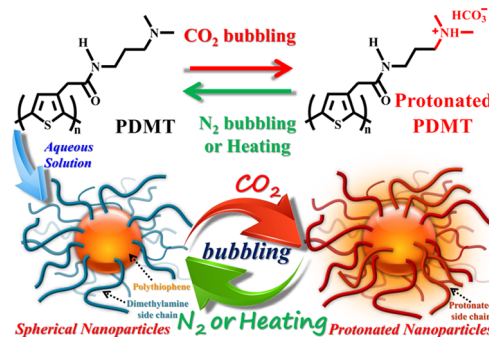
Revised: October 20, 2020

from one state to another, thus gaseous stimulation has received considerable attention among academic researchers in recent years.<sup>33–37</sup> Numerous gas-responsive polymers exhibiting unique physical and chemical properties have been synthesized and intensively investigated in recent years.<sup>38–41</sup> The abundant greenhouse gas carbon dioxide ( $\text{CO}_2$ ) is nontoxic, noncorrosive, and noncombustible, and is commonly used as a trigger stimuli in existing  $\text{CO}_2$ -responsive polymers.<sup>34–37,42</sup> For example, tertiary amine-containing polymers react with  $\text{CO}_2$  to generate charged ammonium bicarbonate in an aqueous solution upon bubbling  $\text{CO}_2$ .<sup>43</sup> When the solution is subsequently heated or purged with inert gases such as nitrogen ( $\text{N}_2$ ) or argon, the ammonium bicarbonate group returns to its original structure, leading to reversible microstructural changes and a hydrophobic–hydrophilic switching phenomenon.<sup>38,43–45</sup> Inspired by these important and desirable properties, subsequent research reports further demonstrated that gas stimuli can control the self-assembly behavior and solubility of WCPs in an aqueous solution and can be used to directly control their fluorescence and amphiphilic properties to form highly reversible fluorescent nanosensors.<sup>46–49</sup> Incorporation of  $\text{CO}_2$ -sensitive functional groups into WCPs may alter their natural characteristics and enable effective modulation of surface charge to achieve stable, hierarchically self-assembled nanostructures in aqueous and biological environments. Therefore, the exploitation of  $\text{CO}_2$ -responsive WCPs as multifunctional nanoprobes for biosensors and bioimaging may hold great promise.

In our previous studies, we found that the amphiphilicity of tertiary amine-containing functional (bio-)polymers could be rapidly switched on and off in an aqueous solution in the presence of  $\text{CO}_2$  and  $\text{N}_2$ , and thus act as emulsifying agents for the separation of oil–water emulsions.<sup>45,50–53</sup> Inspired by these findings, we sought to further explore a facile, highly efficient, inexpensive route for the preparation of functional WCPs with tailorabile physical characteristics on  $\text{CO}_2$  bubbling. We logically speculated that introducing a tertiary amine group into a highly water-soluble fluorescent conjugated polymer may endow  $\text{CO}_2$ -sensitive behavior and enable the creation of high-performance fluorescence nano-objects with the structural stability and fluorescence stability required for bioimaging *in vitro* and *in vivo*. This newly proposed approach could potentially provide a biomedical tool with remarkable multifunctional optical properties for bioimaging and biosensing applications.

Herein, we successfully developed a new oligomeric poly(thiophene) containing pendant tertiary amine groups (hereafter referred to simply as PDMT), which is highly soluble in water and can self-assemble into sphere-like aggregates due to the existence of a repulsive force between the hydrophobic poly(thiophene) backbone and hydrophilic pendant groups (Scheme 1). In addition, the particle size and fluorescence properties of PDMT can be efficiently controlled by  $\text{CO}_2$  bubbling to achieve a high-efficiency fluorescent material, and the fluorescence performance could be restored by repeated  $\text{CO}_2$  and  $\text{N}_2$  bubbling. More importantly, *in vitro* cellular experiments and *in vivo* zebrafish embryo assays demonstrated that bubbling  $\text{CO}_2$  into biomedia containing the PDMT polymer did not lead to cytotoxic effects in the cells or zebrafish larvae, and also remarkably enhanced the cellular internalization and fluorescence stability of the polymers in the intracellular environment and live zebrafish larvae. To the best of our knowledge, this is the first example of a  $\text{CO}_2$  stimuli-

**Scheme 1. Graphical Representation of the Fluorescence Switching Properties of the PDMT Polymer in Response to  $\text{CO}_2$  and  $\text{N}_2$  Bubbling**



responsive WCP for *in vitro* and *in vivo* bioimaging applications that exhibits improved overall structural stability and fluorescent performance after  $\text{CO}_2$  bubbling, which also significantly enhanced the cellular uptake and fluorescence intensity of the WCP both *in vitro* and *in vivo*. Thus, this newly developed WCP system offers a favorable combination of  $\text{CO}_2$  responsiveness, amphiphilic properties, fluorescent behavior, and bioimaging performance, and could represent a multi-functional fluorescent nanoprobe for multiobject tracking in bioimaging and dynamic biological processes.

## ■ EXPERIMENTAL SECTION

**Materials.** All chemicals, solvents, and reagents were of analytical grade and purchased from either TEDIA (Fairfield, OH) or Sigma-Aldrich (St. Louis, MO) and used directly without purification. Nontumor murine fibroblast NIH-3T3 cells and HeLa human cervical cancer cells were obtained from the American Type Culture Collection (Manassas, VA). Reagents and materials for *in vitro* and *in vivo* assays, including phosphate-buffered saline (PBS), Dulbecco's modified Eagle's medium (DMEM), fetal bovine serum (FBS), trypsin with 0.25% ethylenediaminetetraacetic acid (EDTA), penicillin, and streptomycin, were purchased from Invitrogen (Thermo Fisher Scientific, Carlsbad, CA).

**Characterization.** *Proton and Carbon-13 Nuclear Magnetic Resonance* ( $^1\text{H}$  NMR and  $^{13}\text{C}$  NMR). NMR spectra were generated using a multinuclear Bruker AVIII Spectrometer (500 MHz, Fällanden, Switzerland). Approximately 20 mg of samples in deuterated solvent were assessed at 25 °C. The molecular weight distribution of polymer samples in water was analyzed using a matrix-assisted laser desorption/ionization (MALDI) ion source coupled with time-of-flight (TOF) mass spectrometry (MALDI-TOF MS, Bruker, Billerica, MA, USA) in  $\alpha$ -cyano-4-hydroxycinnamic acid (CHCA) as the matrix. Surface charge, hydrodynamic diameter, size distributions and polydispersity index (PDI) of aqueous polymer solutions were obtained with a dynamic light scattering (DLS) instrument (NanoBrook 90Plus PALS, Brookhaven, Holtsville, NY, USA). All samples were incubated at 25 °C at least 30 min before DLS measurements. Scanning electron microscopy (SEM). Polymer samples (0.05 mg) in 1 mL of water were spun onto silicon wafers at 1000 rpm for 30 s, dried under vacuum conditions at 30 °C for 1 day, and viewed using a high-resolution field-emission microscope (JSM-6500F SEM, JEOL, Tokyo, Japan). Ultraviolet–visible (UV–vis) and photoluminescence (PL) spectra were obtained using a UV–vis spectrophotometer (Jasco V-730, Hitachi, Tokyo, Japan) and a PL spectrophotometer (JASCO FP-8300, Hitachi, Tokyo, Japan).

**Synthesis of *N*-(3-(Dimethylamino)propyl)-2-(thiophen-3-yl)acetamide (M1).** Ethyl 3-thiophenecacetate (17.0 g, 0.1 mol) and 3-dimethylaminopropylamine (153.3 g, 1.5 mol) were dissolved in 500 mL of ethanol, and heated to 60 °C with stirring until the carbonyl group of the ester bond at 1725  $\text{cm}^{-1}$  completely disappeared in infrared spectroscopy. Ethanol and 3-dimethylamino-

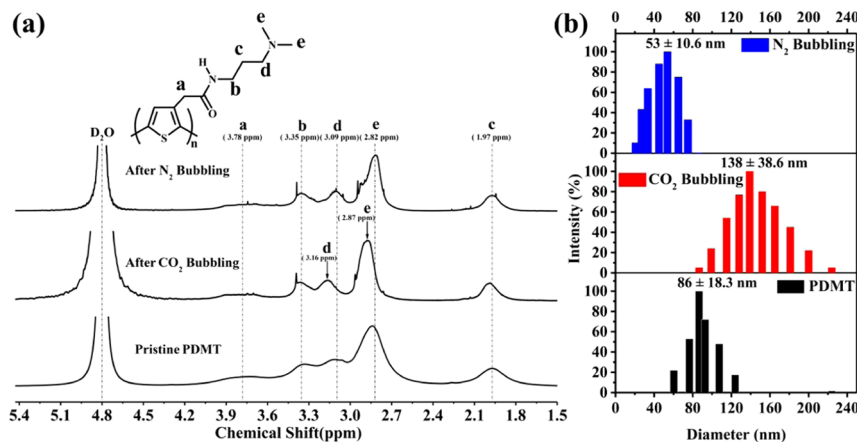


**Figure 1.** (a) <sup>1</sup>H NMR spectra and (b) DLS analyses of aqueous PDMT solutions before and after bubbling CO<sub>2</sub> and N<sub>2</sub> at 25 °C.

propylamine were removed by vacuum distillation, the crude oil sample was dissolved in chloroform, extracted several times in large volumes of deionized water, and the organic layer was collected, dried over anhydrous magnesium sulfate, and filtered. Chloroform was removed by rotary evaporation at 45 °C and the product was dried under vacuum at 30 °C for 1 day to yield a light yellow viscous liquid. Yield: 80% (18.1 g).

**Synthesis of a PDMT Polymer.** M1 (2.0 g, 8.85 mmol) was polymerized with anhydrous ferric chloride (FeCl<sub>3</sub>, 7.0 g, 43.1 mmol) in anhydrous chloroform (80 mL) by stirring for 16 h at 10 °C under a nitrogen atmosphere. The chloroform was removed by rotary evaporation, the solution was purified by dialysis (molecular-weight cutoff, 1000 g/mol) against pure deionized water at 25 °C for 3 days, and the deionized water was removed by vacuum distillation at 45 °C to obtain a red powder. Yield: 48% (0.96 g).

**Cell Culture.** NIH-3T3 fibroblasts or HeLa cells were cultured in DMEM containing 1% penicillin and streptomycin and 10% FBS for 24 h at 37 °C in a humidified atmosphere of 5% CO<sub>2</sub>. Subsequently, the cells were washed with sterile PBS, harvested by trypsinization, and pelleted at 4 °C; the numbers of viable cells were counted by 0.1% trypan blue staining using a light microscope.

**In Vitro Cell Viability Assays.** The biocompatibility of pristine PDMT before and after gas bubbling against NIH-3T3 fibroblasts and HeLa cells was assessed using standard MTT assay protocols, as previously described in detail.<sup>52,63</sup>

**Flow Cytometric Analysis of Fluorescent Pristine and CO<sub>2</sub>-Treated PDMT.** HeLa cells were seeded into six-well plates (approximately 1 × 10<sup>5</sup> cells/well) and incubated with pristine PDMT before and after CO<sub>2</sub> bubbling in PBS (pH 7.4) at 37 °C for 1 or 6 h. Subsequently, cells were washed in PBS, harvested with trypsin and EDTA, and resuspended in PBS. The cellular uptake and distribution of pristine PDMT before and after CO<sub>2</sub> bubbling were analyzed by flow cytometry (FACSAriaTM III; BD Biosciences, San Jose, CA, USA).

**Cellular Uptake of Pristine and CO<sub>2</sub>-Treated PDMT.** HeLa cells were seeded into six-well plates (approximately 1 × 10<sup>5</sup> cells/well) and incubated with pristine or CO<sub>2</sub>-treated PDMT in PBS (pH 7.4) at 37 °C for 1, 3, or 6 h. Subsequently, cells were fixed in 4% formaldehyde, washed twice with PBS, cell nuclei were stained with 4',6-diamidino-2-phenylindole dihydrochloride (DAPI) for 10 min, and the cells were washed several times with PBS and directly observed using an iRIS Digital Cell Imaging System (Logos Bio Systems, Anyang, Korea).

**Confocal Fluorescence Imaging and Biocompatibility of Pristine and CO<sub>2</sub>-Treated PDMT in Living Zebrafish.** Experimental zebrafish were maintained under a 14 h light and 10 h dark cycle at 28 °C and optimal breeding conditions.<sup>64</sup> Subsequently, spawning of eggs was stimulated by light in the morning and started almost immediately following fertilization. After incubation for 2 days, zebrafish were maintained at 28 °C in an E3 embryo medium,<sup>65</sup> and then incubated with 1.0 µg/mL pristine or CO<sub>2</sub>-treated PDMT

nano-particles for 24, 48, or 72 h (72–120 h post fertilization (hpf)) in the E3 medium at 28 °C. After washing several times with the E3 medium to remove the residual PDMT, the zebrafish were directly imaged and traced using a light sheet fluorescence microscope. The fluorescence intensity of the zebrafish was calculated using the image analysis system of TissueGnostics TissueFAXS & HistoFAXS (TissueGnostics GmbH, Vienna, Austria).

To assess the biocompatibility, the survival rates (%) of zebrafish exposed to pristine and CO<sub>2</sub>-treated PDMT for different periods of time were determined using GraphPad Prism 5.0 (GraphPad Software, San Diego, CA), as previously described in detail.<sup>66</sup>

**Statistical Analysis.** The results are presented as the average and standard deviation (SD) of the three independent experiments, each performed in triplicate.

## RESULTS AND DISCUSSION

New tertiary amine-containing oligomeric PDMT was successfully prepared using a simple, efficient two-step reaction process, as presented in Scheme S1 (see the Supporting Information for more details). Briefly, the monomer *N*-(3-(dimethylamino)propyl)-2-(thiophen-3-yl)acetamide (M1) was synthesized through a condensation reaction between ethyl thiophene-3-acetate and 3-(dimethylamino)-1-propylamine using ethanol as a solvent. Subsequently, M1 was further polymerized via ferric chloride-catalyzed oxidative coupling polymerization under low-temperature conditions to obtain the PDMT polymer, the structure of which is illustrated in Scheme 1. After further purification by dialysis, an acceptable yield of PDMT was achieved (~50%), with the resultant polymer exhibiting the expected macromolecular architecture and low molecular weight ( $M_w < 3000$ ; average 12 repeat units), as demonstrated by proton and carbon-13 nuclear magnetic resonance (NMR) spectroscopy (Figures S1–S4) and matrix-assisted laser desorption/ionization time-of-flight mass (MALDI-TOF MS) spectrometry (Figure S5). To explore the influence of CO<sub>2</sub> bubbling on structural transformation and molecular chain movement of the PDMT polymer in an aqueous solution, we performed <sup>1</sup>H NMR of PDMT in deuterated water (D<sub>2</sub>O) before and after bubbling with CO<sub>2</sub> or N<sub>2</sub>. As shown in Figure 1a, after CO<sub>2</sub> bubbling for 60 min at 25 °C, the d and e proton signals of the tertiary amine groups within the PDMT structure dramatically shifted downfield, suggesting that the hydrogen ions (H<sup>+</sup>) and bicarbonate ions (HCO<sub>3</sub><sup>-</sup>) formed on bubbling CO<sub>2</sub> into the solution were associated with the tertiary amine groups in PDMT to produce charged ammonium bicarbonate groups (Scheme 1),<sup>43</sup> thus enhancing the hydrophilic nature of

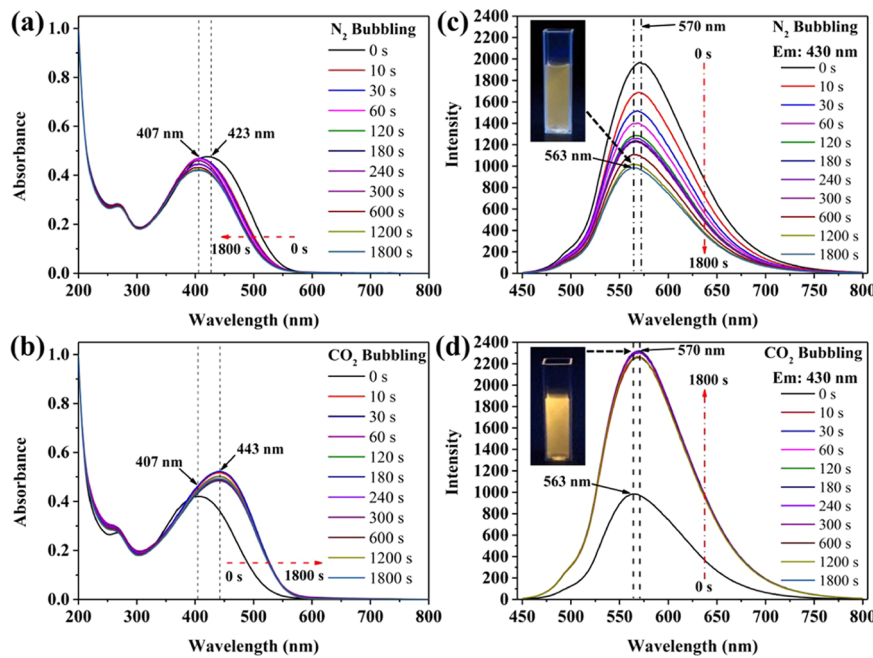


**Figure 2.** (a, b) UV-vis and (c, d) PL spectra of N<sub>2</sub>-treated and CO<sub>2</sub>-treated PDMT polymers in the aqueous solution over time at 25 °C. (c, d) Inset shows N<sub>2</sub>-treated and CO<sub>2</sub>-treated PDMT solutions exposed to ultraviolet light.

PDMT and significantly increasing the repulsive forces between the hydrophobic polythiophene backbone and hydrophilic protonated side chains. However, after bubbling N<sub>2</sub> for 60 min at 25 °C in the same solution previously treated with CO<sub>2</sub>, the proton signals of the tertiary amine groups returned to their original positions, confirming that subsequent N<sub>2</sub> bubbling effectively removed CO<sub>2</sub> from the polymer structure and reversed the transformation into a neutrally charged structure. These results also implied that the amphiphilic characteristics of the water-soluble PDMT polymer undergo reversible changes when bubbled with CO<sub>2</sub> or N<sub>2</sub>. Thus, these interesting findings encouraged us to further investigate the self-assembled structures and fluorescence characteristics of PDMT in aqueous environments.

To obtain further insight into the self-assembly behavior of PDMT in an aqueous solution before and after CO<sub>2</sub> bubbling, we carried out dynamic light scattering (DLS) and scanning electron microscopy (SEM) at 25 °C. At an aqueous sample concentration of 0.1 mg/mL, DLS revealed that PDMT had an average diameter of 86 ± 18.3 nm (PDI = 0.132) with an average  $\zeta$ -potential of -16.72 ± 1.17 mV (Figure 1b), indicating that the presence of hydrophobic tertiary amine groups in PDMT led to formation of nanosized objects. This result also may be attributed to generation of amphiphilic repulsive forces between the hydrophobic polythiophene backbone and hydrophilic tertiary amine side chains of PDMT, which lead to formation of phase-separated nanoaggregates.<sup>34</sup> Interestingly, after bubbling CO<sub>2</sub> for 60 min, the average diameter and  $\zeta$ -potential of CO<sub>2</sub>-treated PDMT changed significantly to 138 ± 38.6 nm (PDI = 0.198) and -27.46 ± 0.92 mV, respectively, indicating that CO<sub>2</sub> bubbling remarkably affected the self-assembled structural characteristics and surface charge of PDMT due to formation of charged ammonium bicarbonate in the polymer side chains, which induced larger, aggregated structures. However, after bubbling N<sub>2</sub> for 60 min into the solution previously treated with CO<sub>2</sub>, the average diameter and  $\zeta$ -potential of PDMT reverted back

to a “neutral/nonionic state” (i. e., average diameter = 53 ± 10.6 nm, PDI = 0.126 and  $\zeta$ -potential = -16.3 ± 0.78 mV), indicating the particle size and surface charge of PDMT undergo reversible changes after bubbling and releasing CO<sub>2</sub> in the aqueous solution. Notably, N<sub>2</sub>-treated PDMT had a smaller average diameter of (53 ± 10.6 nm) than pristine PDMT (86 ± 18.3 nm), which could possibly be attributed to a certain extent of destruction/relaxation of aggregates on N<sub>2</sub> bubbling, resulting in a smaller particle size. In other words, these intriguing results seem likely that the change in particle size and  $\zeta$ -potential was directly caused by a change in the degree of the protonation and deprotonation of the amine moieties after CO<sub>2</sub> and N<sub>2</sub> bubbling. Further insight into the changes in the morphology and particle size of PDMT in an aqueous solution after CO<sub>2</sub> and N<sub>2</sub> bubbling was obtained through scanning electron microscopy (SEM). As presented in Figure S6, the particle sizes of the PDMT polymer before and after bubbling CO<sub>2</sub> and N<sub>2</sub> determined by SEM were consistent with the DLS results (Figure 1b). Before and after N<sub>2</sub> bubbling, PDMT exhibited irregular sphere-like morphologies, a rather loose structure, and particle sizes smaller than 50 nm (Figure S6a,b). In contrast, after CO<sub>2</sub> bubbling, PDMT formed dense, well-defined spheres larger than 100 nm (Figure S6c), implying that CO<sub>2</sub> bubbling promoted aggregation of the polymer nanoparticles, thus enhancing the particle interactions and size. In other words, the process of CO<sub>2</sub> bubbling in an aqueous PDMT solution may promote the occurrence of phase separation between the hydrophobic polythiophene backbone and charged ammonium bicarbonate moieties, thus leading to increased particle size and  $\zeta$ -potential. In addition, the SEM further confirmed that the particle sizes of the PDMT nanoparticles change reversibly upon CO<sub>2</sub> and N<sub>2</sub> bubbling.

To identify the optimal concentration of PDMT for ultraviolet-visible (UV-vis) and fluorescence studies, the concentration-dependent effects in an aqueous solution were studied by photoluminescence (PL) spectroscopy at concentrations ranging from 0.5 to 0.01 mg/mL. PDMT had the

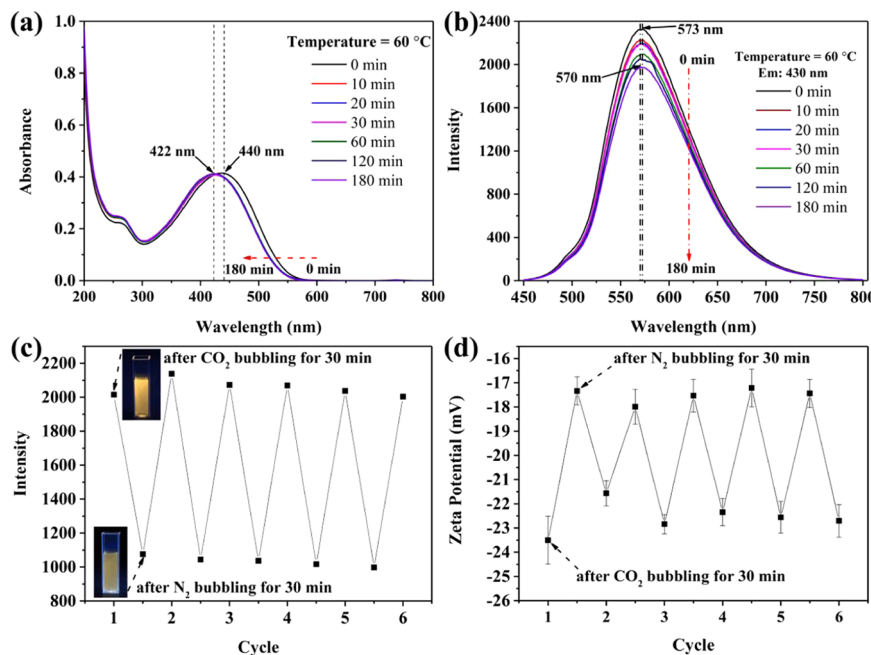


**Figure 3.** (a) UV-vis and (b) PL spectra of N<sub>2</sub>-treated and CO<sub>2</sub>-treated PDMT polymers in the aqueous solution over time at 60 °C. (c) Reversible changes in fluorescence intensity and the (d)  $\zeta$ -potential of the PDMT polymer in water upon CO<sub>2</sub> and N<sub>2</sub> treatment. (c) Insets show the N<sub>2</sub>-treated and CO<sub>2</sub>-treated PDMT solutions exposed to ultraviolet light.

highest fluorescence intensity at 560 nm at 0.04 mg/mL, whereas lower concentrations exhibited lower fluorescence intensities (Figure S7). When the concentration was gradually increased from 0.04 to 0.5 mg/mL, the fluorescence intensity of PDMT gradually decreased, and completely disappeared at 0.5 mg/mL, implying that aggregation at high concentrations quenched the fluorescence of the conjugated polymer.<sup>55</sup> The concentration of 0.04 mg/mL PDMT in an aqueous solution was selected as the optimal balance between high fluorescence intensity and sample concentration for further studies of the CO<sub>2</sub>-responsive characteristics of PDMT (Figure S7). UV-vis and PL measurements were performed at 25 °C to further explore the effect of CO<sub>2</sub> bubbling on the fluorescent properties of the PDMT polymer in an aqueous solution. As shown in the UV-vis spectra in Figure 2a, the maximum absorbance peak of PDMT gradually blue-shifted from 423 to 407 nm as N<sub>2</sub> was continuously bubbled into the polymer solution over 0–1800 s at 25 °C. This blue-shift phenomenon could possibly be attributed to disentanglement of the polymer chains within the nanoparticles on N<sub>2</sub> bubbling. Surprisingly, after bubbling CO<sub>2</sub> for 0–1800 s at 25 °C into the solution previously treated with N<sub>2</sub>, the maximum absorbance peak of PDMT gradually red-shifted from 407 to 443 nm (Figure 2b) and had a higher intensity compared to pristine PDMT before and after bubbling with N<sub>2</sub>. The red shift and enhanced intensity induced by introducing large amounts of charged ammonium bicarbonate groups into the nanoparticle structures on bubbling CO<sub>2</sub> may be attributed to formation of aggregates and charge-induced hydrophilic–hydrophobic phase separation between the nanoparticles. Similar results were observed in the fluorescence spectra. As shown in Figure 2c, the maximum fluorescence wavelength of PDMT at 570 nm gradually decreased in intensity and shifted slightly to 563 nm after N<sub>2</sub> bubbling for 1800 s, indicating N<sub>2</sub> bubbling effectively weakened intermolecular aggregation of PDMT, leading to a less restrained polymeric conformation and lower fluorescence

intensity. CO<sub>2</sub> was subsequently bubbled into the solution treated with N<sub>2</sub>. Surprisingly, after bubbling CO<sub>2</sub> for only 10 s, the intensity and position of the maximum fluorescence peaks of PDMT increased and rapidly red-shifted from 982 to 2330 and from 563 to 570 nm, respectively (Figure 2d), representing a 2.3-fold increase in fluorescence intensity compared to N<sub>2</sub>-treated PDMT. Further extending the CO<sub>2</sub> bubbling time from 10 to 1800 s only slightly further increased the intensity values from 2260 to 2330, indicating that CO<sub>2</sub> rapidly reacts with PDMT to produce ammonium bicarbonate groups in an aqueous solution, resulting in significantly different and distinct characteristics in the UV-vis and PL spectra and macroscopic fluorescence brightness before and after bubbling CO<sub>2</sub> and N<sub>2</sub> (as indicated by the inset pictures in Figure 2c,d). In addition, these observations support our hypothesis that the fluorescence properties of CO<sub>2</sub>- and N<sub>2</sub>-responsive PDMT nanoparticles can be efficiently manipulated to achieve tunable wavelength and brightness. Thus, these unique phenomena peaked our curiosity to explore the fluorescence stability and reversibility of PDMT in an aqueous solution.

To further understand the influence of environmental temperature on the structural stability of CO<sub>2</sub>-responsive conjugated polymers, PDMT aqueous solutions were bubbled with CO<sub>2</sub> for 30 min at 25 and 60 °C and assessed by UV-vis and PL spectroscopies. At 25 °C, the fluorescence intensity of PDMT only slightly decreased from 3070 to 2887 over 168 h of monitoring (Figure S8a), suggesting that the CO<sub>2</sub>-absorbed PDMT polymer possesses exceptional fluorescence properties and long-term structural stability. Based on Figure S8a, the activation energy ( $E_a$ ) of CO<sub>2</sub> desorption from PDMT was calculated to be 2.04 kJ/mol using the Arrhenius equation (Figure S8b),<sup>56</sup> which is much lower than the previously reported  $E_a$  values for amine-based CO<sub>2</sub> capture materials,<sup>56–58</sup> possibly due to the lower molecular weight of PDMT. The UV-vis and PL spectra of PDMT significantly altered when

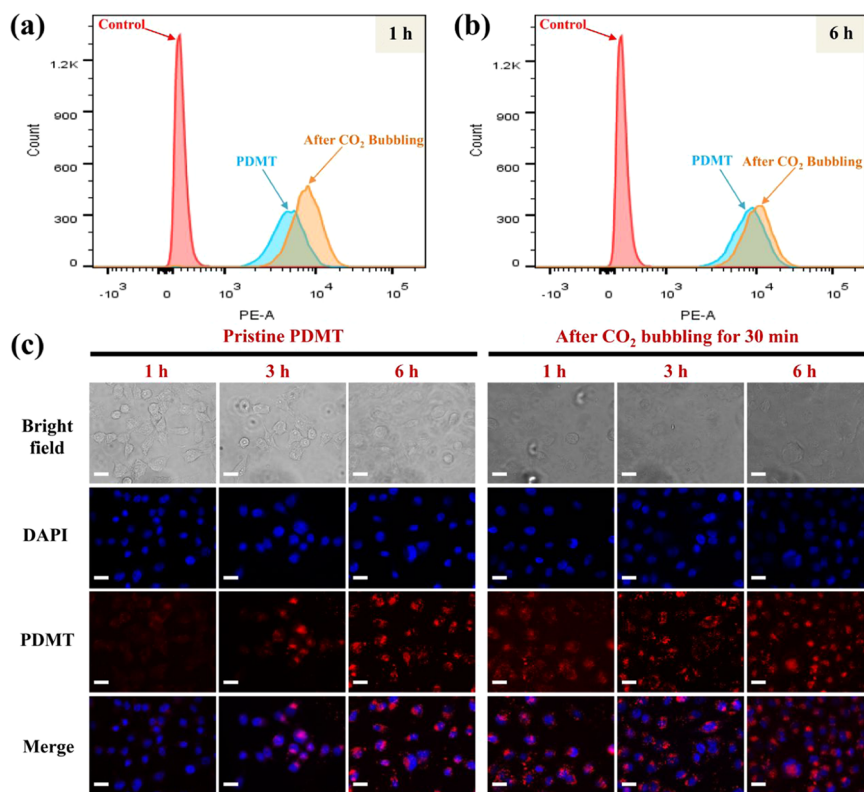


**Figure 4.** (a, b) Flow cytometric analysis and (c) CLSM images of HeLa cells incubated with pristine or  $\text{CO}_2$ -treated PDMT polymers at pH 7.4 and 37 °C for different periods of time. Scale bars are 20  $\mu\text{m}$  for all CLSM images.

the environmental temperature was increased to 60 °C (Figure 3a,b). After heating at 60 °C for only 180 min, the maximal wavelengths of both spectra exhibited blue shifts, while the intensity of the fluorescence peak gradually decreased (from 2325 to 1972) over time (Figure 3b), indicating that increasing the temperature accelerated the removal of  $\text{CO}_2$  from PDMT—to the extent that the original structural state gradually recovered. In other words,  $\text{CO}_2$ -treated PDMT in an aqueous solution exhibited remarkably higher structural stability at 25 °C than at 60 °C, further confirming that the rate of  $\text{CO}_2$  removal from the PDMT nanoparticles was directly proportional to the temperature.

Next, we assessed whether the gas-controlled fluorescence characteristics of PDMT nanoparticles could be reversibly regenerated by  $\text{CO}_2$  and  $\text{N}_2$  bubbling cycles to markedly improve the stability of the fluorescence switching properties and explore the potential of PDMT as a fluorescent probe for biological applications. Cyclic performance on alternating  $\text{CO}_2$  and  $\text{N}_2$  bubbling was directly evaluated by carrying out PL and  $\zeta$ -potential measurements (Figure 3c,d). Over six cycles of  $\text{CO}_2$  and  $\text{N}_2$  bubbling, an aqueous PDMT solution underwent noticeable gas-dependent stimulation and the fluorescence intensity reverted back to almost the original value after each cycle of  $\text{N}_2$  bubbling, indicating a connection between the fluorescence and optical switching properties (Figure 3c). Similarly, the  $\zeta$ -potential of PDMT in an aqueous solution reversibly and stably switched between  $-17.5$  mV after  $\text{N}_2$  bubbling and  $-22.5$  mV after  $\text{CO}_2$  bubbling (Figure 3d). This suggests that the intermolecular associations between the polymeric structures and  $\text{CO}_2$  molecules induce a unique structural transition from a neutral structure to a form of charged ammonium bicarbonate when  $\text{CO}_2$  was bubbled into

the aqueous PDMT solution, even though PDMT can form sphere-like, nanosized structures. Thus, these observations demonstrate that the fluorescence switching characteristics of the  $\text{CO}_2$ - and  $\text{N}_2$ -responsive PDMT polymer maintain excellent reversibility in an aqueous solution, and that its structural charge characteristics can be rapidly and reversibly manipulated by alternating  $\text{CO}_2$  and  $\text{N}_2$  bubbling. To date, there are no reports of a  $\text{CO}_2$ -responsive WCP system that possesses reversibly controllable chemical and physical properties in an aqueous solution upon  $\text{CO}_2$  and  $\text{N}_2$  treatments.

Based on these findings, we boldly speculated that the  $\text{CO}_2$ -responsive PDMT nanoparticles exhibit enhanced fluorescence properties in an aqueous solution and could potentially be used in *in vitro* and *in vivo* biological imaging applications to achieve fluorescence images with high contrast and stability. *In vitro* cell viability evaluations were carried out using the methyl thiazolyl tetrazolium (MTT) colorimetric test in nontumor murine fibroblast NIH-3T3 cells and human cervical cancer cells (HeLa). After 24 h of incubation at 37 °C and 5%  $\text{CO}_2$ , neither  $\text{CO}_2$ -bubbled nor  $\text{N}_2$ -bubbled PDMT solutions at concentrations ranging from 0.01 to 20  $\mu\text{g}/\text{mL}$  had significant cytotoxic effects on normal NIH-3T3 or HeLa cancer cells (Figures S9 and S10). In addition,  $\text{CO}_2$  and  $\text{N}_2$  bubbling did not affect cell viability. To understand whether PDMT nanoparticles (both before and after  $\text{CO}_2$  bubbling) can act as highly stable and efficient fluorescent probes to enhance cellular internalization and achieve high-resolution fluorescent bioimaging of cell tracking; the cellular internalization and intracellular distribution of the nanoparticles were analyzed in HeLa cells by flow cytometry. As shown in Figure 4a,b, compared to cells cultured with pristine PDMT nanoparticles at pH 7.4 for 1 or 6 h, the red fluorescence observed in the

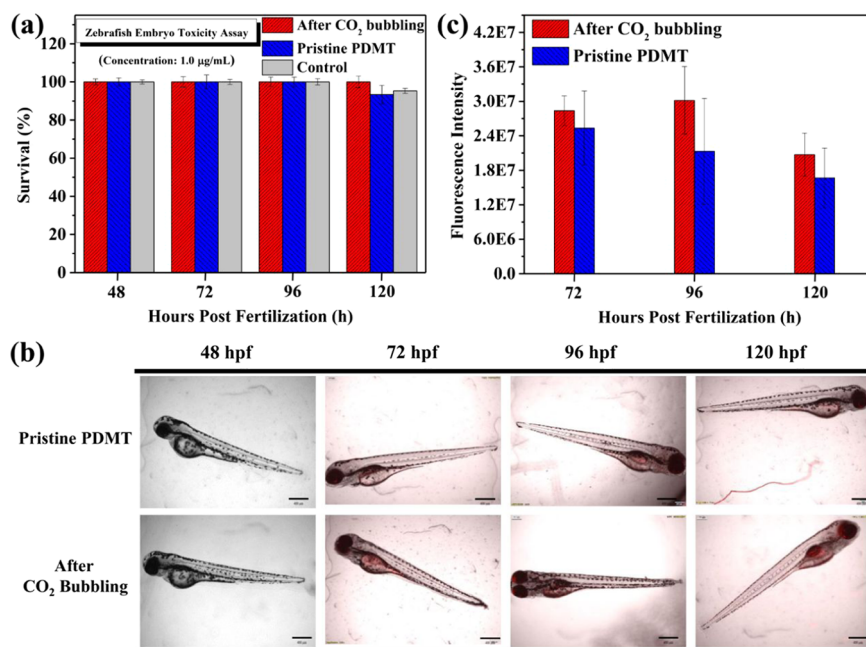


**Figure 5.** (a) Survival rates of zebrafish embryos exposed to 1.0 µg/mL pristine or CO<sub>2</sub>-treated PDMT nanoparticles for different periods of time. (b) Fluorescence microscopy images of zebrafish treated with PDMT nanoparticles before and after bubbling CO<sub>2</sub> into the culture media for different periods of time. All scale bars = 400 µm. (c) Plot of the fluorescence intensities of pristine and CO<sub>2</sub>-treated PDMT nanoparticles in living zebrafish over time.

intracellular region of HeLa cells cultured with CO<sub>2</sub>-treated PDMT nanoparticles shifted dramatically to a higher fluorescence intensity, implying that the CO<sub>2</sub>-bubbled PDMT nanoparticles achieved enhanced cellular internalization in HeLa cells, which, in turn, improved the intracellular fluorescence intensity. The enhanced cellular uptake also implies that their surface charge enabled the CO<sub>2</sub>-treated nanoparticles to interact with the cell surface to enhance cellular association and internalization of the nanoparticles within the HeLa cells and influence the distribution of the nanoparticles in the intracellular environment.

To verify the results of the flow cytometry assays, confocal laser scanning microscopy (CLSM) was used to determine the internalization rate and intracellular distribution of PDMT before and after CO<sub>2</sub> bubbling. As presented in Figure 4c, the blue fluorescent dye 4'-6-diamidino-2-phenylindole (DAPI) was used to specifically stain cell nuclei and the distribution of PDMT in cells was indicated by red fluorescence. After incubation with pristine PDMT for 1 h, the CLSM images only revealed a weak distribution of red fluorescence on the outer surface of the cell membrane and almost no pink regions indicating colocalization of PDMT with the HeLa cell nuclei. These results suggest that pristine PDMT exhibited a slow rate of cellular internalization at the beginning of the incubation period. In contrast, when HeLa cells were cultured with CO<sub>2</sub>-treated PDMT nanoparticles (after 30 min CO<sub>2</sub> bubbling) for 1 h, strong bright red and pink fluorescence were observed in the cytoplasm and nuclei of the HeLa cells, respectively. After a prolonged incubation of 3 or 6 h, the brightness of both fluorescent colors within the cells remarkably increased compared to cells cultured with the CO<sub>2</sub>-treated nanoparticles for 1 h, which is in good agreement with the flow cytometry results (Figure 4a,b). These results indicate that the CO<sub>2</sub>-treated PDMT nanoparticles efficiently passed through the cell membrane and the nucleus and exhibited improved

fluorescence stability and endocytic efficiency under cellular conditions compared to pristine PDMT due to tuning of the surface charge of the nanoparticles by CO<sub>2</sub> treatment. In other words, bubbling an aqueous solution of PDMT with CO<sub>2</sub> is a critical factor that affects the cellular uptake and fluorescence performance of PDMT nanoparticles in cells *in vitro*, thus PDMT holds great potential for bioimaging and long-term tracking *in vivo*.

Next, we explored the fluorescence characteristics of CO<sub>2</sub>-treated PDMT nanoparticles for bioimaging and long-term observations *in vivo*. *In vivo* toxicity assays are the first important step toward determining the biocompatibility of fluorescent probes. A zebrafish model was employed to evaluate the toxicity of PDMT nanoparticles *in vivo* before and after CO<sub>2</sub> bubbling. Zebrafish (48 hpf) were incubated with 1.0 µg/mL pristine or CO<sub>2</sub>-treated PDMT nanoparticles in embryo media at 28 °C for 3 days. As shown in Figure 5a, zebrafish cultured with PDMT nanoparticles (both before and after CO<sub>2</sub> bubbling) exhibited high survival rates, suggesting that CO<sub>2</sub>-responsive PDMT possesses low cytotoxicity and high biocompatibility in zebrafish, and thus is potentially suitable for a wide variety of biological applications.<sup>16,17,59–61</sup> In addition, introduction of charged ammonium bicarbonate groups into PDMT did not affect the zebrafish survival rates. Next, to further examine the fluorescent distribution and brightness and contrast of PDMT in zebrafish, 48 hpf zebrafish were incubated with pristine or CO<sub>2</sub>-treated PDMT nanoparticles for different periods of time at 28 °C and fluorescence images were captured using a fluorescence microscope. As shown in Figure 5b, no fluorescence was observed in untreated zebrafish at 48 h after hatching. Subsequently, when 48 hpf zebrafish were incubated with pristine or CO<sub>2</sub>-treated PDMT nanoparticles for 3 days (72–120 hpf), a bright red fluorescence was detected in several tissues, indicating that the PDMT nanoparticles rapidly and efficiently entered the

zebrafish and exhibited a red fluorescence in living bodies *via* an obvious turn-on fluorescence response. Interestingly, fluorescence analysis of accurate automated quantitative imaging clearly showed that zebrafish incubated with CO<sub>2</sub>-treated PDMT nanoparticles displayed significantly higher mean fluorescence intensities than zebrafish cultured with pristine PDMT at each culture stage (Figure 5c), implying that CO<sub>2</sub> treatment dramatically improved the fluorescence performance of PDMT in living zebrafish. Notably, the fluorescence intensities gradually increased with the culture time, with maximum fluorescence intensity observed at 96 hpf, indicating the CO<sub>2</sub>-treated nanoparticles exhibited structural stability and remarkable fluorescence enhancement in zebrafish. However, the fluorescence intensity of zebrafish cultured with CO<sub>2</sub>-treated nanoparticles significantly reduced when the culture time was extended to 120 hpf, possibly due to a decrease in the fluorescence intensity due to the release of some CO<sub>2</sub> from the PDMT. In contrast, the fluorescence intensity of zebrafish incubated with pristine PDMT decreased linearly over time (Figure 5c), further confirming that CO<sub>2</sub> bubbling not only maintained the biocompatibility of PDMT nanoparticles in zebrafish but also greatly improved the quality and stability of *in vivo* fluorescence imaging. Thus, this new class of CO<sub>2</sub>-responsive WCP could be potentially used as a multifunctional fluorescent probe to advance *in vivo* biological imaging applications.

## CONCLUSIONS

In summary, we developed a simple, facile method to efficiently synthesize CO<sub>2</sub>-responsive PDMT as a fluorescent stimuli-sensitive fluorescence probe that is suitable for a variety of potential *in vitro* and *in vivo* biological imaging applications. Owing to the presence of hydrophilic and CO<sub>2</sub>-responsive tertiary amine moieties in the side chains of the polymer, PDMT spontaneously self-assembles into a sphere-like nanoaggregate in an aqueous solution, possesses interesting amphiphilic, optical, and photoluminescence properties, and exhibits extremely low cytotoxicity toward normal and tumor cells. Furthermore, the structural charge and fluorescence properties of the PDMT nanoparticles can be rapidly and reversibly manipulated by alternate CO<sub>2</sub> and N<sub>2</sub> bubbling, which results in significantly enhanced fluorescence and surface-charge switching properties and a stable cyclic on and off response. In addition, *in vitro* cellular internalization and CLSM images demonstrated that CO<sub>2</sub> bubbling substantially improved the cellular uptake of the CO<sub>2</sub>-treated PDMT nanoparticles and subsequently enhanced their fluorescence intensity, distribution, and endocytic efficiency within the cellular environment compared to pristine PDMT. Importantly, *in vivo* zebrafish assays revealed that CO<sub>2</sub>-treated PDMT nanoparticles exhibited good biocompatibility and remarkable fluorescence enhancement *in vivo*, whereas the fluorescence brightness and photostability of pristine PDMT decreased linearly over time. The combination of these important features is critical for a WCP-based nanoparticle system that is suitable as a multifunctional fluorescent probe for *in vivo* cellular imaging. Overall, the present work provides a rapid, highly effective route to exploit the unique controllable CO<sub>2</sub>-responsive characteristics of tertiary amine-functionalized WCP nanoparticles in an aqueous solution to control the fluorescence properties and internalization ability of the nanoparticles *in vitro* and *in vivo*, and demonstrates the high

potential ability of this system for both biological and clinical imaging applications.

## ASSOCIATED CONTENT

### Supporting Information

The Supporting Information is available free of charge at <https://pubs.acs.org/doi/10.1021/acs.biomac.0c01336>.

The synthesis procedure, <sup>1</sup>H and <sup>13</sup>C NMR spectra, mass data, elemental analysis, the MALDI-TOF mass spectrum, SEM images, PL results, and cell viability assays (PDF)

## AUTHOR INFORMATION

### Corresponding Author

Chih-Chia Cheng – Graduate Institute of Applied Science and Technology and Advanced Membrane Materials Research Center, National Taiwan University of Science and Technology, Taipei 10607, Taiwan; [orcid.org/0000-0002-1605-6338](https://orcid.org/0000-0002-1605-6338); Email: [cccheng@mail.ntust.edu.tw](mailto:cccheng@mail.ntust.edu.tw)

### Authors

You-Cheng Lai – Graduate Institute of Applied Science and Technology, National Taiwan University of Science and Technology, Taipei 10607, Taiwan

Yeong-Tarng Shieh – Department of Chemical and Materials Engineering, National University of Kaohsiung, Kaohsiung 81148, Taiwan; [orcid.org/0000-0002-6306-6643](https://orcid.org/0000-0002-6306-6643)

Yi-Hsuan Chang – Graduate Institute of Applied Science and Technology, National Taiwan University of Science and Technology, Taipei 10607, Taiwan

Ai-Wei Lee – Department of Anatomy and Cell Biology, School of Medicine, College of Medicine and Taipei Heart Institute, Taipei Medical University, Taipei 11031, Taiwan; Cardiovascular Research Center, Taipei Medical University Hospital, Taipei 11031, Taiwan

Jem-Kun Chen – Department of Materials Science and Engineering, National Taiwan University of Science and Technology, Taipei 10607, Taiwan

Duu-Jong Lee – Department of Chemical Engineering, National Taiwan University of Science and Technology, Taipei 10607, Taiwan; Department of Chemical Engineering, National Taiwan University, Taipei 10617, Taiwan; [orcid.org/0000-0002-8820-8097](https://orcid.org/0000-0002-8820-8097)

Juin-Yih Lai – Graduate Institute of Applied Science and Technology and Advanced Membrane Materials Research Center, National Taiwan University of Science and Technology, Taipei 10607, Taiwan; R&D Center for Membrane Technology, Chung Yuan Christian University, Taoyuan 32043, Taiwan

Complete contact information is available at:

<https://pubs.acs.org/10.1021/acs.biomac.0c01336>

### Author Contributions

Y.-C.L. carried out all experiments. Y.-T.S. provided critical suggestions on the experiments of gas responsiveness. Y.-H.C. helped in the synthesis and biological experiments. C.-C.C. conceived the original idea, designed the experiments, processed the experimental data, and wrote the paper. All authors discussed the results and provided constructive comments to the final version of the paper.

### Notes

The authors declare no competing financial interest.

## ACKNOWLEDGMENTS

This study was supported financially by the Ministry of Science and Technology, Taiwan (contract no. MOST 107-2221-E-011-041-MY3) and the National Taiwan University of Science and Technology—Taipei Medical University Joint Research Program (contract no. NTUST-TMU-109-03).

## REFERENCES

- (1) Knecht, U.; Woitowitz, H. J. Human Toxicokinetics of Inhaled Monochlorobenzene: Latest Experimental Findings Regarding Re-evaluation of the Biological Tolerance Value. *Int. Arch. Occup. Environ. Health* **2000**, *73*, 543–554.
- (2) Cao, W.; Xue, J. Recent Progress in Organic Photovoltaics: Device Architecture and Optical Design. *Energy Environ. Sci.* **2014**, *7*, 2123–2144.
- (3) Chi, D.; Qu, S.; Wang, Z.; Wang, J. High Efficiency P3HT:PCBM Solar Cells with an Inserted PCBM Layer. *J. Mater. Chem. C* **2014**, *2*, 4383–4387.
- (4) Huang, F.; Wu, H.; Cao, Y. Water/Alcohol Soluble Conjugated Polymers as Highly Efficient electron Transporting/Injection Layer in Optoelectronic Devices. *Chem. Soc. Rev.* **2010**, *39*, 2500–2521.
- (5) Feng, X.; Liu, L.; Wang, S.; Zhu, D. Water-Soluble Fluorescent Conjugated Polymers and Their Interactions with Biomacromolecules for Sensitive Biosensors. *Chem. Soc. Rev.* **2010**, *39*, 2411–2419.
- (6) Feng, L.; Zhu, C.; Yuan, H.; Liu, L.; Lv, F.; Wang, S. Conjugated Polymer Nanoparticles: Preparation, Properties, Functionalization and Biological Applications. *Chem. Soc. Rev.* **2013**, *42*, 6620–6633.
- (7) Das, S.; Routh, P.; Ghosh, R.; Chatterjee, D. P.; Nandi, A. K. Water-Soluble Ionic Polythiophenes for Biological and Analytical Applications. *Polym. Int.* **2017**, *66*, 623–639.
- (8) Braeken, Y.; Cheruku, S.; Ethirajan, A.; Maes, W. Conjugated Polymer Nanoparticles for Bioimaging. *Materials* **2017**, *10*, 1420.
- (9) McCullough, R. D.; Ewbank, P. C.; Loewe, R. S. Self-Assembly and Disassembly of Regioregular, Water Soluble Polythiophenes: Chemoselective Ionchromatic Sensing in Water. *J. Am. Chem. Soc.* **1997**, *119*, 633–634.
- (10) Polavarapu, L.; Xu, Q.-H. Water-Soluble Conjugated Polymer-Induced Self-Assembly of Gold Nanoparticles and Its Application to SERS. *Langmuir* **2008**, *24*, 10608–10611.
- (11) Chai, R.; Xing, C.; Qi, J.; Fan, Y.; Yuan, H.; Niu, R.; Zhan, Y.; Xu, J. Water-Soluble Conjugated Polymers for the Detection and Inhibition of Protein Aggregation. *Adv. Funct. Mater.* **2016**, *26*, 9026–9031.
- (12) Huang, Y.-Q.; Zhang, R.; Zhao, Y.-K.; Chen, H.; Jiang, R.-C.; Liu, X.-F.; Fan, Q.-L.; Wang, L.-H.; Huang, W. Self-Assembled Nanoparticles Based on a Cationic Conjugated Polymer/Hyaluronan–Cisplatin Complex as a Multifunctional Platform for Simultaneous Tumor-Targeting Cell Imaging and Drug Delivery. *New J. Chem.* **2017**, *41*, 4998–5006.
- (13) Traina, C. A.; Bakus, R. C., II; Bazan, G. C. Design and Synthesis of Monofunctionalized, Water-Soluble Conjugated Polymers for Biosensing and Imaging Applications. *J. Am. Chem. Soc.* **2011**, *133*, 12600–12607.
- (14) Pu, K.-Y.; Liu, B. Fluorescent Conjugated Polyelectrolytes for Bioimaging. *Adv. Funct. Mater.* **2011**, *21*, 3408–3423.
- (15) Qian, C.-G.; Zhu, S.; Feng, P.-J.; Chen, Y.-L.; Yu, J.-C.; Tang, X.; Liu, Y.; Shen, Q.-D. Conjugated Polymer Nanoparticles for Fluorescence Imaging and Sensing of Neurotransmitter Dopamine in Living Cells and the Brains of Zebrafish Larvae. *ACS Appl. Mater. Interfaces* **2015**, *7*, 18581–18589.
- (16) Zhou, L.; Lv, F.; Liu, L.; Wang, S. Water-Soluble Conjugated Organic Molecules as Optical and Electrochemical Materials for Interdisciplinary Biological Applications. *Acc. Chem. Res.* **2019**, *52*, 3211–3222.
- (17) Wang, Y.; Feng, L.; Wang, S. Conjugated Polymer Nanoparticles for Imaging, Cell Activity Regulation, and Therapy. *Adv. Funct. Mater.* **2019**, *29*, No. 1806818.
- (18) Brendel, J. C.; Schmidt, M. M.; Hagen, G.; Moos, R.; Thelakkat, M. Controlled Synthesis of Water-Soluble Conjugated Polyelectrolytes Leading to Excellent Hole Transport Mobility. *Chem. Mater.* **2014**, *26*, 1992–1998.
- (19) Kuehne, A. J. C. Conjugated Polymer Nanoparticles toward *In Vivo* Theranostics – Focus on Targeting, Imaging, Therapy, and the Importance of Clearance. *Adv. Biosys.* **2017**, *1*, No. 1700100.
- (20) Huang, B.; Geng, Z.; Yan, S.; Li, Z.; Cai, J.; Wang, Z. Water-Soluble Conjugated Polymer as a Fluorescent Probe for Monitoring Adenosine Triphosphate Level Fluctuation in Cell Membranes during Cell Apoptosis and *In Vivo*. *Anal. Chem.* **2017**, *89*, 8816–8821.
- (21) Lu, X.; Yuan, P.; Zhang, W.; Wu, Q.; Wang, X.; Zhao, M.; Sun, P.; Huang, W.; Fan, Q. A Highly Water-Soluble Triblock Conjugated Polymer for *In Vivo* NIR-II Imaging and Photothermal Therapy of Cancer. *Polym. Chem.* **2018**, *9*, 3118–3126.
- (22) Stuart, M. A. C.; Huck, W. T. S.; Genzer, J.; Muller, M.; Ober, C.; Stamm, M.; Sukhorukov, G. B.; Szleifer, I.; Tsukruk, V. V.; Urban, M.; Winnik, F.; Zauscher, S.; Luzinov, I.; Minko, S. Emerging Applications of Stimuli-Responsive Polymer Materials. *Nat. Mater.* **2010**, *9*, 101–113.
- (23) Yan, X.; Wang, F.; Zheng, B.; Huang, F. Stimuli-Responsive Supramolecular Polymeric Materials. *Chem. Soc. Rev.* **2012**, *41*, 6042–6065.
- (24) Feng, A. C.; Yuan, J. Y. Smart Nanocontainers: Progress on Novel Stimuli-Responsive Polymer Vesicles. *Macromol. Rapid Commun.* **2014**, *35*, 767–779.
- (25) Wei, M.; Gao, Y.; Li, X.; Serpe, M. J. Stimuli-Responsive Polymers and Their Applications. *Polym. Chem.* **2017**, *8*, 127–143.
- (26) Abdollahi, A.; Roghani-Mamaqani, H.; Razavi, B. Stimuli-Chromism of Photoswitches in Smart Polymers: Recent Advances and Applications as Chemosensors. *Prog. Polym. Sci.* **2019**, *98*, No. 101149.
- (27) Weber, C.; Hoogenboom, R.; Schubert, U. S. Temperature Responsive Bio-Compatible Polymers Based on Poly(ethylene oxide) and Poly(2-oxazoline)s. *Prog. Polym. Sci.* **2012**, *37*, 686–714.
- (28) Jochum, F. D.; Theato, P. Temperature- and Light-Responsive Smart Polymer Materials. *Chem. Soc. Rev.* **2013**, *42*, 7468–7483.
- (29) Kocak, G.; Tuncer, C.; Büttün, V. pH-Responsive Polymers. *Polym. Chem.* **2017**, *8*, 144–176.
- (30) Tang, H.; Zhao, W.; Yu, J.; Li, Y.; Zhao, C. Recent Development of pH-Responsive Polymers for Cancer Nanomedicine. *Molecules* **2019**, *24*, No. 4.
- (31) Bertrand, O.; Gohy, J. F. Photo-Responsive Polymers: Synthesis and Applications. *Polym. Chem.* **2017**, *8*, 52–73.
- (32) Thévenota, J.; Oliveiraa, H.; Sandre, O.; Lecommandoux, S. Magnetic Responsive Polymer Composite Materials. *Chem. Soc. Rev.* **2013**, *42*, 7099–7116.
- (33) Yan, Q.; Zhao, Y. Block Copolymer Self-Assembly Controlled by the “Green” Gas Stimulus of Carbon Dioxide. *Chem. Commun.* **2014**, *50*, 11631–11641.
- (34) Darabi, A.; Jessop, P. G.; Cunningham, M. F. CO<sub>2</sub>-Responsive Polymeric Materials: Synthesis, Self-Assembly, and Functional Applications. *Chem. Soc. Rev.* **2016**, *45*, 4391–4436.
- (35) Zhang, Q.; Lei, L.; Zhu, S. Gas-Responsive Polymers. *ACS Macro Lett.* **2017**, *6*, 515–522.
- (36) Liu, H.; Lin, S.; Feng, Y.; Theato, P. CO<sub>2</sub>-Responsive Polymer Materials. *Polym. Chem.* **2017**, *8*, 12–23.
- (37) Jiang, B.; Zhang, Y.; Huang, X.; Kang, T.; Severtson, S. J.; Wang, W.-J.; Liu, P. Tailoring CO<sub>2</sub>-Responsive Polymers and Nanohybrids for Green Chemistry and Processes. *Ind. Eng. Chem. Res.* **2019**, *58*, 15088–15108.
- (38) Zhang, Q.; Zhu, S. Oxygen and Carbon Dioxide Dual Responsive Nanoaggregates of Fluoro- and Amino-Containing Copolymer. *ACS Macro Lett.* **2014**, *3*, 743–746.
- (39) Park, J.; Pramanick, S.; Park, D.; Yeo, J.; Lee, J.; Lee, H.; Kim, W. J. Therapeutic-Gas-Responsive Hydrogel. *Adv. Mater.* **2017**, *29*, No. 1702859.

- (40) Wang, Y.; Huo, M.; Zeng, M.; Liu, L.; Ye, Q.-Q.; Chen, X.; Li, D.; Peng, L.; Yuan, J. CO<sub>2</sub>-responsive Polymeric Fluorescent Sensor with Ultrafast Response. *Chin. J. Polym. Sci.* **2018**, *36*, 1321–1327.
- (41) Chen, L.; Liu, R.; Yan, Q. Polymer Meets Frustrated Lewis Pair: Second-Generation CO<sub>2</sub>-Responsive Nanosystem for Sustainable CO<sub>2</sub> Conversion. *Angew. Chem.* **2018**, *130*, 9480–9484.
- (42) Li, Y.; Zhu, L.; Grishkewich, N.; Tam, K. C.; Yuan, J.; Mao, Z.; Sui, X. CO<sub>2</sub>-Responsive Cellulose Nanofibers Aerogels for Switchable Oil–Water Separation. *ACS Appl. Mater. Interfaces* **2019**, *11*, 9367–9373.
- (43) Fan, W.; Tong, X.; Farnia, F.; Yu, B.; Zhao, Y. CO<sub>2</sub>-Responsive Polymer Single-Chain Nanoparticles and Self-Assembly for Gas-Tunable Nanoreactors. *Chem. Mater.* **2017**, *29*, 5693–5701.
- (44) Mihara, M.; Jessop, P. G.; Cunningham, M. F. Redispersible Polymer Colloids Using Carbon Dioxide as an External Trigger. *Macromolecules* **2011**, *44*, 3688–3693.
- (45) Shieh, Y.-T.; Lin, Y.-T.; Cheng, C.-C. CO<sub>2</sub>-Switchable Behavior of Chitosan-g-Poly[(2-Dimethylamino)Ethylmethacrylate] as an Emulsifier. *Carbohydr. Polym.* **2017**, *170*, 281–288.
- (46) Fan, Y.; Xing, C.; Yuan, H.; Chai, R.; Zhao, L.; Zhan, Y. Conjugated Polyelectrolyte-Based New Strategy for in Situ Detection of Carbon Dioxide. *ACS Appl. Mater. Interfaces* **2017**, *9*, 20313–20317.
- (47) Yuan, H.; Xing, C.; Fan, Y.; Chai, R.; Niu, R.; Zhan, Y.; Peng, F.; Qi, J. Carbon Dioxide-Controlled Assembly of Water-Soluble Conjugated Polymers Catalyzed by Carbonic Anhydrase. *Macromol. Rapid Commun.* **2017**, *38*, No. 1600726.
- (48) Byun, J.; Huang, W.; Wang, D.; Li, R.; Zhang, K. A. I. CO<sub>2</sub>-Triggered Switchable Hydrophilicity of a Heterogeneous Conjugated Polymer Photocatalyst for Enhanced Catalytic Activity in Water. *Angew. Chem., Int. Ed.* **2018**, *57*, 2967–2971.
- (49) Wang, B.; Xing, C.; Gao, D.; Yuan, H.; Qiu, L.; Yang, X.; Huang, Y.; Zhan, Y. Carbon Dioxide-Controlled Assembly Based on Conjugated Polymer and Boron Nitride. *Chin. Chem. Lett.* **2020**, *31*, 261–264.
- (50) Shieh, Y. T.; Hu, F. Z.; Cheng, C. C. CO<sub>2</sub>-Switchable Multi-Stimuli-Responsive Polymer Nanoparticle Dispersion. *ACS Appl. Nano Mater.* **2018**, *1*, 384–393.
- (51) Shieh, Y. T.; Tai, P. Y.; Cheng, C. C. Dual CO<sub>2</sub>/Temperature-Responsive Diblock Copolymers Confer Controlled Reversible Emulsion Behavior. *Polym. Chem.* **2019**, *10*, 2641–2646.
- (52) Shieh, Y. T.; Tai, P. Y.; Cheng, C. C. Polymer Nanoparticles with A Sensitive CO<sub>2</sub>-Responsive Hydrophilic/Hydrophobic Surface. *J. Polym. Sci., Part A: Polym. Chem.* **2019**, *57*, 2149–21562150.
- (53) Shieh, Y. T.; Yeh, Y. C.; Cheng, C. C. Two-Way CO<sub>2</sub>-Responsive Polymer Particles with Controllable Amphiphilic Properties. *ACS Omega* **2020**, *5*, 1862–1869.
- (54) Cheng, C. C.; Lin, W. L.; Liao, Z. S.; Chu, C. W.; Huang, J. J.; Huang, S. Y.; Fan, W. L.; Lee, D. J. Water-Soluble Fullerene-Functionalized Polymer Micelles for Efficient Aqueous-Processed Conductive Devices. *Polym. Chem.* **2017**, *8*, 7469–7474.
- (55) Yuan, W. Z.; Lu, P.; Chen, S.; Lam, J. W. Y.; Wang, Z.; Liu, Y.; Kwok, H. S.; Ma, Y.; Tang, B. Z. Changing the Behavior of Chromophores from Aggregation-Caused Quenching to Aggregation-Induced Emission: Development of Highly Efficient Light Emitters in the Solid State. *Adv. Mater.* **2010**, *22*, 2159–2163.
- (56) Teng, Y.; Liu, Z.; Xu, G.; Zhang, K. Desorption Kinetics and Mechanisms of CO<sub>2</sub> on Amine-Based Mesoporous Silica Materials. *Energies* **2017**, *10*, No. 115.
- (57) Wang, J.; Huang, L.; Yang, R.; Zhang, Z.; Wu, J.; Gao, Y.; Wang, Q.; O'Hare, D.; Zhong, Z. Recent Advances in Solid Sorbents for CO<sub>2</sub> Capture and New Development Trends. *Energy Environ. Sci.* **2014**, *7*, 3478–3518.
- (58) Didas, S. A.; Choi, S.; Chaikittisilp, W.; Jones, C. W. Amine-Oxide Hybrid Materials for CO<sub>2</sub> Capture from Ambient Air. *Acc. Chem. Res.* **2015**, *48*, 2680–2687.
- (59) Peng, H.-S.; Chiu, D. T. Soft Fluorescent Nanomaterials for Biological and Biomedical Imaging. *Chem. Soc. Rev.* **2015**, *44*, 4699–4722.
- (60) Ke, C.-S.; Fang, C.-C.; Yan, J.-Y.; Tseng, P.-J.; Pyle, J. R.; Chen, C.-P.; Lin, S.-Y.; Chen, J.; Zhang, X.; Chan, Y.-H. Molecular Engineering and Design of Semiconducting Polymer Dots with Narrow-Band, Near-Infrared Emission for *In Vivo* Biological Imaging. *ACS Nano* **2017**, *11*, 3166–3177.
- (61) Zeglio, E.; Rutz, A. L.; Winkler, T. E.; Malliaras, G. G.; Herland, A. Conjugated Polymers for Assessing and Controlling Biological Functions. *Adv. Mater.* **2019**, *31*, No. 1806712.
- (62) Cheng, C. C.; Liang, M. C.; Liao, Z. S.; Huang, J. J.; Lee, D. J. Self-Assembled Supramolecular Nanogels as A Safe and Effective Drug Delivery Vector for Cancer Therapy. *Macromol. Biosci.* **2017**, *17*, No. 1600370.
- (63) Liao, Z. S.; Huang, S. Y.; Huang, J. J.; Chen, J. K.; Lee, A. W.; Lai, J. Y.; Lee, D. J.; Cheng, C. C. Self-Assembled pH-Responsive Polymeric Micelles for Highly Efficient, Non-Cytotoxic Delivery of Doxorubicin Chemotherapy to Inhibit Macrophage Activation: *In Vitro* Investigation. *Biomacromolecules* **2018**, *19*, 2772–2781.
- (64) Hou, J. T.; Yang, J.; Li, K.; Yu, K. K.; Yu, X. Q. A Colorimetric and Red Emissive Fluorescent Probe for Cysteine and Its Application in Bioimaging. *Sens. Actuators, B* **2015**, *214*, 92–100.
- (65) Mu, X.; Pang, S.; Sun, X.; Gao, J.; Chen, J.; Chen, X.; Li, X.; Wang, C. Evaluation of Acute and Developmental Effects of Difenoconazole via Multiple Stage Zebrafish Assays. *Environ. Pollut.* **2013**, *175*, 147–157.
- (66) Gao, X.-P.; Feng, F.; Zhang, X.-Q.; Liu, X.-X.; Wang, Y.-B.; She, J.-X.; He, Z.-H.; He, M.-F. Toxicity Assessment of 7 Anticancer Compounds in Zebrafish. *Int. J. Toxicol.* **2014**, *33*, 98–105.